U.D.C. 621.3.083.2 : 513.42

Study of the Location of Transition Metal Cations in Synthetic Zeolites Using Electron Paramagnetic Resonance and Optical Spectroscopy

I.D.Mikheikin, G.M.Zhidomirov, and V.B.Kazanskii

The application of EPR and optical reflection spectroscopy to the study of zeolites containing first-row transition metal cations is discussed. A qualitative theoretical analysis of the optical and magnetic properties of some ions with an unfilled $(d)^n$ electron shell is given. The most important results of EPR and reflection spectroscopic studies of the behaviour of transition metal cations in synthetic zeolites are presented. 80 references

CONTENTS

I. Introduction 468
II. Calculations of the optical and magnetic properties of first-row transition metal ions in low-symmetry ligand fields 470
III. Results of studies on zeolites containing metal ions of the first transition row 473

I. INTRODUCTION

Synthetic zeolites are widely used for the separation of hydrocarbons by adsorption, for drying gases, and in petroleum refining. The last application is particularly important, because zeolites containing bi- and trivalent metal cations (introduced by cation exchange) are much more active catalysts than the amorphous aluminosilicates previously used. Most workers ascribe the catalytic properties of cation-exchanged zeolites to the polyvalent ions themselves, or to acidic centres formed by the introduction of these ions into the crystal lattice. Hence, location studies of polyvalent metal ions in synthetic zeolite structures are of fundamental importance in understanding their catalytic properties.

Because of the large volume of publications on various properties of zeolites, including a number of contradictory statements, special review articles have been written on the catalytic activity of zeolites[1-4], on the state of water and other molecules adsorbed by zeolites[5], and other similar topics. Some of these reviews discuss the location of polyvalent cations within the lattice, mainly on the basis of structural studies of zeolites containing alkali, alkaline-earth, and rare-earth metal ions.

An attempt is made here to systematise the published results of work on the structure of zeolites containing transition-metal ions. The number of such publications is not large, but it is sufficient to show that zeolites containing transition-metal cations have catalytic properties essentially different from those of zeolites containing alkali or alkaline-earth metal ions. A special feature of the present review is that conclusions regarding the sites occupied by transition-metal cations are drawn entirely from the results of optical and EPR spectral studies of the zeolites. The discussion will be largely confined to zeolites containing cations of the first transition group (ions with an unfilled 3*d* electron shell). The theory of the EPR and optical spectra of these ions is sufficiently well understood, and the spectral results can be interpreted with confidence in the light of the wealth of experimental information on homogeneous complexes. Zeolites containing cations of other transition metals have not so far been investigated by EPR and optical spectroscopy.

1. General Discussion of Synthetic Zeolites and Cation Localisation Sites in their Crystal Lattices

Zeolites, both naturally occurring and synthetic, are crystalline aluminosilicates†. The various forms of zeolites have been described in detail elsewhere, and we shall therefore only briefly consider the properties of zeolites with a three-dimensional skeletal structure, which have the highest adsorption capacity and thermal stability and therefore offer the greatest promise in the field of catalysis. Among the three-dimensional skeletal zeolites, we shall be concerned in particular with the recently developed and widely used synthetic zeolites of types A, X, and Y. The skeleton of these zeolites consists of aluminium–oxygen and silicon–oxygen tetrahedra. Twenty-four of these tetrahedra are joined to form a polyhedron (cubo-octahedron), and the cubo-octahedra are joined by oxygen bridges into the crystalline skeleton of the zeolite. Depending on the aluminium to silicon ratio, these zeolites fall into three types: A ($SiO_2/Al_2O_3 = 2$), X ($SiO_2/Al_2O_3 = 2.2-3$), and Y ($SiO_2/Al_2O_3 = 3.2-5.0$).

In type A zeolites the cubo-octahedra form a simple cubic lattice, similar to the rocksalt structure, but with each ion replaced by a cubo-octahedron. The cubo-octahedra are connected by four-membered oxygen bridges (see Fig. 1*a*). In zeolites of types X and Y the cubo-octahedra are arranged in a lattice of the diamond type, and the bridges connecting the cubo-octahedra consist of six oxygen atoms (see Fig. 1*b*).

Because of their skeletal structure, the zeolites contain holes which are interconnected by windows of well defined sizes. The holes within the cubo-octahedra are termed small holes, and their size is practically the same in zeolites A, X, and Y ($v = 150$ Å^3, $d = 6.5$ Å). The hollows bounded by the outer surfaces of the cubo-octahedra and of the oxygen bridges are termed large zeolite holes. Their diameter in A, X, and Y zeolites is ~ 11.5Å,

† Zeolites have been synthesised in which the aluminium is replaced by gallium[6,7], or chromium[8,9], and the silicon is replaced by germanium[6], beryllium, or magnesium[10].

and their volume is of the order of 800 Å^3.[11] The diameter of the six-membered oxygen windows leading from the small to the large holes is approximately 2 Å. In type-A zeolites the large holes are interconnected by 8-membered oxygen windows ($d \simeq 4.2$ Å), and in zeolites of types X and Y by 12-membered oxygen windows 8–9 Å in diameter.

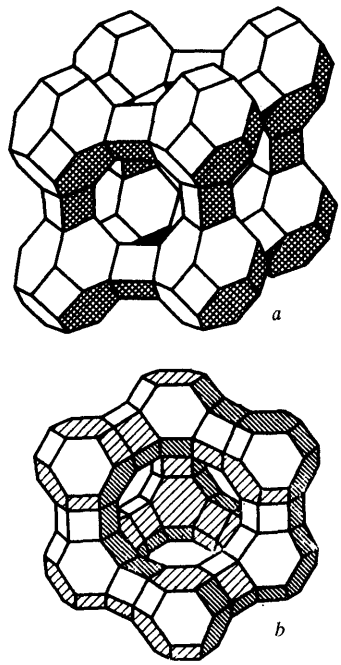


Figure 1. Three-dimensional model of the alumina–silica lattice of zeolites (*a*) of type A and (*b*) of types X and Y.

Since the aluminium–oxygen tetrahedra carry an excess of negative charge, the zeolite structure must include an equivalent amount of metal cations (usually Na^+ or Ca^{2+}). These ions can readily be exchanged[12] by other ions, and therefore a great variety of cationic forms of zeolite can be prepared. Without discussing cation exchange in detail, we note in passing that the process is determined by the nature of the metal ions, their size and charge, the pH of the medium, the temperature, and the structure of the zeolite[13–19]. The crystal lattice parameters of the zeolite are not significantly altered by cation exchange, up to the point where the crystal lattice breaks down. The stability of the zeolite structure towards exchange is determined mainly by the pH of the medium, the extent of exchange, and the zeolite type.

One of the most important problems in the structure of cationic zeolite forms concerns the sites occupied by the metal ions which compensate the charge on the aluminium–oxygen tetrahedra. In zeolites of types X and Y, three types of cation site are usually distinguished[20]: *S*I sites are the centres of the hexagonal prisms formed by the oxygen connecting links between cubo-octahedra (16 sites per unit cell); *S*II sites are the hexagonal oxygen windows which connect the large and the small holes (32 sites per unit cell); *S*III sites are the walls of the channels interconnecting the large holes (48 sites per unit cell). In type-A zeolites the *S*I sites are absent. The differences between the sites which can be occupied by cations have recently been identified in greater detail. Sites in the six-membered oxygen windows adjacent to a large hole have been designated *S*II, those adjacent to a small hole *S*II′. The location of an ion within a small zeolite hole near a six-membered oxygen window leading to the cavity of a hexagonal oxygen prism (*S*I site) is referred to as an *S*I′ site. Some characteristics of the sodium forms of synthetic type A, X, and Y zeolites are listed in Table 1.

Table 1. Some characteristics of the Na-forms of synthetic zeolites (types A, X, Y).

Zeolite type	Composition of the elementary cell of the hydrated zeolite	Size of windows, Å	Population of sites by univalent cations			Lattice parameters, Å	Adsorption capacity for water of 1 g of dehydrated zeolite
			I	II	III		
A	$Na_{12}[(AlO_2)_{12}(SiO_2)_{12}]\cdot 27H_2O$	4.2	—	8	4	12.32	0.30
X	$Na_{86}[(AlO_2)_{86}(SiO_2)_{106}]\cdot 264H_2O$	8.0	16	32	38	24.95	0.36
Y	$Na_{56}[(AlO_2)_{56}(SiO_2)_{136}]\cdot 264H_2O$	8.0	16	32	8	24.70	0.35

The sites available for cations in zeolites of types X and Y are shown schematically in Fig. 2. Depending on the symmetry of the surroundings, two types of site can be distinguished: those with C_{4v} and those with C_{3v} symmetry.

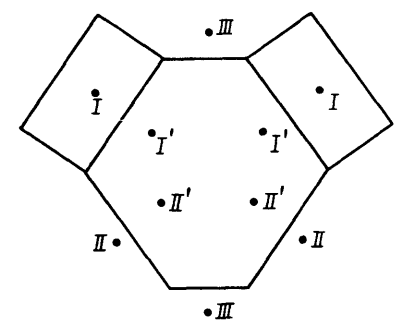


Figure 2. Structure of type X and Y zeolites (diagrammatic). The points show possible localisation sites for ions.

We know from X-ray diffraction studies of zeolites that the hexagonal oxygen windows of the cubo-octahedra are trigonally distorted. They consist of two unequal equilateral triangles, rotated by 60°, formed by the oxygen atoms of the lattice. The interplanar spacing of these triangles is several tens of angstroms.

As a result, the electrical ligand field for cations in *S*I′, *S*II′, and *S*II sites has C_{3v} symmetry (trigonal, compressed or extended along the trigonal axis of the tetrahedron depending on the conditions of the particular

system). The three planar ligands, in this case, are the oxygen atoms of the lattice, and the fourth ligand could be either a residual water molecule (or its fragments O^{2-} or OH^-), or any other adsorbate molecule. When a cation is localised in the plane of the six-membered oxygen window it experiences a ligand field with D_{3h} symmetry (special case of C_{3v}). However, an environment corresponding to a trigonally distorted octahedron can be realised also by the adsorption of three fairly small molecules on a cation in an *S*II position (see below).

The ligand field surrounding *S*I and *S*II sites has a distorted octahedral symmetry. In the former, the ligands are 6 negatively charged oxygen atoms from the zeolite lattice, which form a fairly regular octahedron. (These sites are not accessible to adsorbed molecules.) When a cation is localised on the surface of a large zeolite hole (site *S*III), one or more (up to 4) of the ligands can be provided by the lattice oxygen atoms, and the remainder may be residual water molecules, or other molecules. As will be shown below, the environment of delocalised cations ("floating" in the large holes) of fully hydrated zeolites is almost perfectly octahedral.

2. Basic Physicochemical Methods of Studying Zeolite Structure. Application of EPR and Reflection Optical Spectroscopy to the Study of Zeolites Containing Cations of the First Transition Series

Almost all the physicochemical methods used in the study of heterogeneous catalysts have been applied to the study of zeolite structures. X-ray diffraction and infrared spectroscopy are the most widely used spectroscopic methods. Other methods include chemical analysis, calorimetry, thermogravimetry, differential thermal analysis, electrical and dielectric measurements, tracer studies, measurements of static magnetism, etc. Some problems have been studied by a combination of these methods, with satisfactory results.

X-ray analysis gives the most direct indication of the sites in which metal cations are localised in zeolites, but the results are difficult to interpret because sufficiently large single crystals are not yet available, and powder patterns are exceedingly complicated. Furthermore, the method becomes unreliable at relatively low concentrations of added cations, when these do not give rise to a distinct sublattice. Adsorption and desorption phenomena on cationated zeolite forms are not easily studied by X-ray diffraction. Hence, the usefulness of the X-ray method is limited essentially to studies of the distribution of cations in zeolites.

I. r. spectroscopy is used in the main to study the nature of the acidic centres and the state of the surface hydroxyl groups in zeolites. Its relevance to studies of cation localisation sites stems from the perturbation of the vibrational spectra of adsorbed molecules (e.g. CO) by interaction with cations[21]; this provides information on the accessibility to adsorbed molecules of cations on various sites.

When the zeolite contains ions of transition metals, which are usually paramagnetic and absorb in the u.v. and visible regions of the spectrum, the combined application of EPR and reflection spectroscopy has given very promising results. The EPR and the optical spectra of transition-metal ions are very sensitive to the symmetry of their immediate environment. Hence, the localisation of ions in various crystal lattice sites can be identified, since these sites can be distinguished by the symmetry of their surroundings.

The EPR and optical spectroscopy methods are to some extent complementary, since the splitting of the electronic levels of the ions by the crystal field can easily be determined by the optical method, and the parameters of the EPR spectra are dependent on this splitting. It should be noted, however, that the EPR method gives best results with magnetically dilute samples, containing low concentrations of paramagnetic ions. On the other hand, the optical spectra of such samples tend to be insufficiently intense, owing to the low extinction coefficients of the transition-metal ions. Hence, combined EPR–optical spectral measurements is far from universally applicable.

The interpretation of optical and EPR spectra for transition-metal ions requires a knowledge of the energy levels of the ions and of the corresponding electronic wave functions in ligand fields of different symmetries. Qualitative and semi-quantitative interpretations of EPR and optical effects are usually attempted with the help of ligand-field theory, whose limitations and methods are discussed in detail elsewhere (see, for example, Refs. 22 and 23).

Most of the problems, however, concern small distortions of octahedral and tetrahedral fields, and their solution relies on the application of perturbation theory. Large distortions, e.g. the removal of an entire ligand from the coordination sphere, are not considered as a rule. Therefore, before reviewing the published data, we shall briefly summarise the results of our calculations of the electronic levels and spin-Hamiltonian constants for ions with a $(3d)^n$ electron shell in low-symmetry ligand fields. These calculations allow us to interpret more reliably the EPR and optical spectra of transition-metal cations in zeolites, and they can also be applied to the interpretation of corresponding data for oxide catalysts, on whose surface the coordination of ions may be abnormal[24]. The calculations are directly relevant, also, to the structure of "atypical" complexes of transition metals with structurally complex ligands. For example, in the bivalent copper complex $[Cu(tren)OH]^+$, studied in our laboratory[25], the ligand field has C_3 symmetry, whereas weakly distorted octahedral and tetrahedral structures are more usual for copper.

II. CALCULATIONS OF THE OPTICAL AND MAGNETIC PROPERTIES OF FIRST-ROW TRANSITION METAL IONS IN LOW-SYMMETRY LIGAND FIELDS

A full account of our qualitative evaluation of energy levels and spin-Hamiltonian constants for ions with a $(3d)^n$ electronic configuration in low-symmetry ligand fields lies beyond the scope of the present review. However, our subsequent discussion of experimental results by EPR and optical spectroscopy methods for zeolites containing first-row transition metal cations will be made more meaningful by a brief examination of the following types of ligand field distortion, which (as already stated) are found in zeolites:

1. Tetragonal distortions of a ligand field with O_h symmetry (regular octahedron), including the transition to a square planar symmetry by gradual removal of the two ligands on one of the tetrad axes, and also to axial symmetry by gradual removal of the 4 ligands in the plane perpendicular to the tetrad axis (Fig. 3*a*).

2. Distortions of a trigonal bipyramid, analogous to the above (Fig. 3*b*).

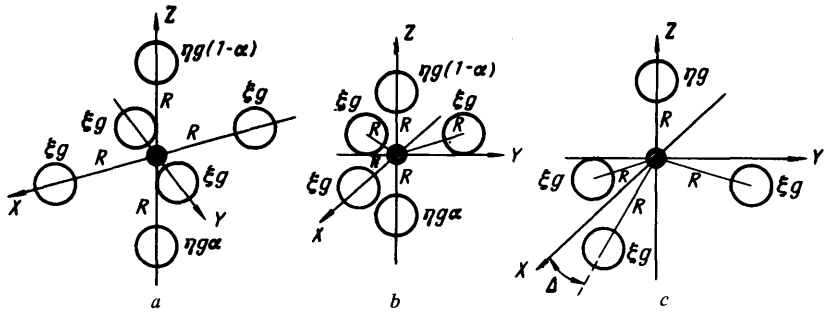


Figure 3. Models of complexes with different symmetry: (*a*) C_{4v}, (*b*) C_{3v} pyram, and (*c*) C_{3v} tetr. ξg is the effective charge on the ligands in the plane; $\eta g(1-\alpha)$ and $\eta g\alpha$ $(0 \leq \alpha \leq 1)$ are the effective charges on the ligands located on the Z axis.

3. Distortions of a tetrahedron (type C_{3v}), including the continuous transition from a planar triangular configuration to a tetrahedron compressed along the trigonal axis (Fig. 3*c*).

These distortions in the ligand field are modelled by varying the charges on the ligands located on the z-axis $[\eta q(1-\alpha)$ and $\eta q\alpha]$ or in the xy plane $[\xi q]$, and also by varying the angle Δ between the planar ligand M and the xy plane (see Fig. 3). The distances between the central ion and all the ligands are assumed to be identical and equal to R.

We shall consider only the special cases of strong and weak ligand field, because the intermediate field approximation requires electronic computation and is usually confined to specific ions in fields of known symmetry.

Ligand fields are termed weak if they split the ground state by an amount smaller than the distance to the nearest excited state but greater than the spin–orbital interaction constant λ for the corresponding ions.

Tables 2 and 3 show the angular components of the electronic wave functions, and expressions for the corresponding eigenvalues of the energy, for the strong and the weak field case respectively, calculated by the ligand field theory[22,23]. The parameters ξ, η, and $\sin^2\Delta$ have already been defined (see Fig. 3); the quantities F_2 and F_4 are the coulombic interaction integrals between an electron localised at the central ion and the spherical harmonics of a ligand field of the second and the fourth order respectively (see Ref. 23 for a more detailed discussion).

The electronic energy levels of ions in the above fields are shown in Figs. 4 and 5. The plots are constructed for $F_4/F_2 = 0.15$ because this case exemplifies nearly all possible intersections of the resulting electronic levels. Similar plots for different values of the ratio F_4/F_2 can easily be made by reference to Tables 2 and 3.

The $(3d)^n$ electron configuration (n = 2, 3, ..., 9) in a strong crystal field is obtained by progressive population of the states derived by us for a single $3d$ electron, with account being taken of Pauli's principle.

The energy levels of transition-metal ions in the free state follow Hund's rule, and therefore the following high-spin states are chosen as the initial levels in the weak field approximation of the ligand field theory:

Configuration	Ground state	Spin	Angular Momentum	Ion
d^1, d^9	^2D	$^1/_2$	2	Ti^{+3}, V^{4+}, Cr^{5+}, Cu^{2+}, Mn^{6+}
d^4, d^6	^5D	2	2	Cr^{2+}, Fe^{2+}, Co^{3+}, Mn^{3+}
d^3, d^7	^4F	$^3/_2$	3	Cr^{3+}, Co^{2+}, V^{2+}
d^2, d^8	^3F	1	3	Cr^{4+}, Ni^{2+}, Co^{+}, V^{3+}
d^5	^6S	$^5/_2$	0	Mn^{2+}, Fe^{3+}

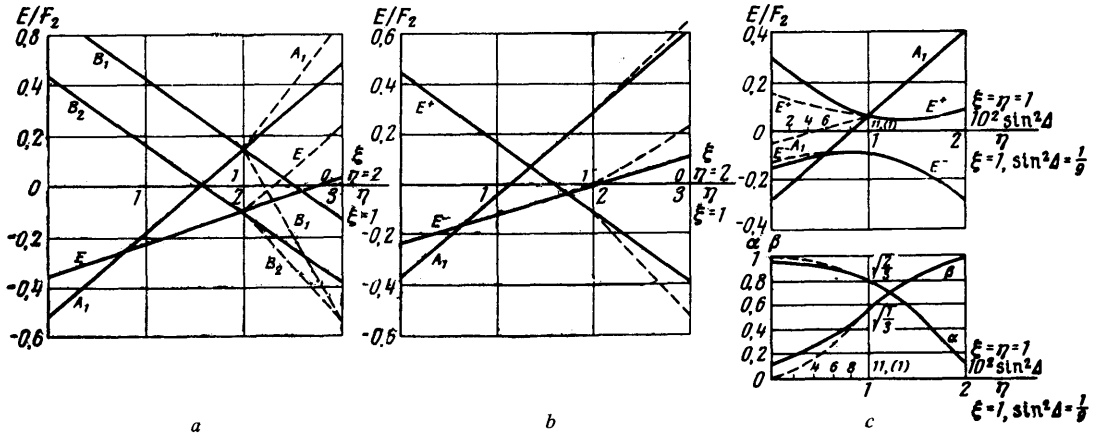


Figure 4. Energy levels of one $3d$ electron in ligand fields of symmetry (*a*) C_{4v}, (*b*) C_{3v} pyram, and (*c*) C_{3v} tetr in units of F_2 $(F_4/F_2 = 0.15)$. Plots of the coefficients in the wave functions are also shown in Fig. 4*c*. The full lines refer to changes in the parameter η at constant $\xi = 1$ (*a*, *b*) or $\xi = 1$, $\Delta = \Delta_{tetr}$; the broken lines refer to changes in the parameter ξ at constant $\eta = 2$ (*a*, *b*) or to changes in the parameter $\sin^2\Delta$ at constant $\xi = \eta = 1$ (*c*).

Table 2. Angular components of the wave functions and corresponding eigenvalues of the energy for one $3d$ electron in electrical ligand fields of symmetry C_{4v}, C_{3v} pyram, and C_{3v} tetr.

C_{4v}			$C_{3v\ pyram}$			$C_{3v\ tetr}$		
Symbol	Ψ	E	Symbol	Ψ	E	Symbol	Ψ	E
A_1	Y_2^0	$2a_2+2a_4$	A_1	Y_2^0	$2a_2+2a_4$	A_1	Y_2^0	$2a_2+2a_4$
B_1	$\frac{1}{\sqrt{2}}\left(Y_2^2+Y_2^{-2}\right)$	$-2a_2+\frac{1}{3}a_4+b$	E^-	$\frac{1}{\sqrt{2}}\left(Y_2^1\pm Y_2^{-1}\right)$	$a_2-\frac{4}{3}a_4$	E^-	$\beta Y_2^2+\alpha Y_2^{-1}$ $\beta Y_2^{-2}-\alpha Y_2^1$	$-\frac{a_2+a_4}{2}-\sqrt{h}$
B_2	$\frac{1}{\sqrt{2}}\left(Y_2^2-Y_2^{-2}\right)$	$-2a_2+\frac{1}{3}a_4-b$	E^+	$\frac{1}{\sqrt{2}}\left(Y_2^2\pm Y_2^{-2}\right)$	$-2a_2+\frac{1}{3}a_4$	E^+	$\alpha Y_2^2-\beta Y_2^{-1}$ $\alpha Y_2^{-2}+\beta Y_2^1$	$-\frac{a_2+a_4}{2}+\sqrt{h}$
E	$\frac{1}{\sqrt{2}}\left(Y_2^1\pm Y_2^{-1}\right)$	$a_2-\frac{4}{3}a_4$						
$a_2=\frac{1}{7}F_2(-2\xi+\eta)$; $b=\frac{5}{6}F_4\xi$; $a_4=\frac{1}{7}F_4\left(\frac{3}{2}\xi+\eta\right)$.			$a_2=\frac{1}{7}F_2\left(-\frac{3}{2}\xi+\eta\right)$; $a_4=\frac{1}{7}F_4\left(\frac{9}{8}\xi+\eta\right)$.			$a_2=\frac{1}{7}F_2\left[\left(-\frac{3}{2}+\frac{9}{2}\sin^2\Delta\right)\xi+\eta\right]$; $a_4=\frac{1}{7}F_4\left[(35\sin^4\Delta-30\sin^2\Delta+3)\frac{3}{8}\xi+\eta\right]$; $h=\left(\frac{a_2+a_4}{2}\right)^2+c^2+2a_2^2+\frac{4}{9}a_4^2-3a_2a_4$; $c^2=\frac{25}{16}\sin^2\Delta\cdot\cos^2\Delta\cdot F_4^2\xi^2$.		

*In Tables 2 and 3 the quantities F_2 and F_4 are taken to be positive. The sign of the product of the unit electronic charge and of unit charge on the ligand is included in the tabulated values of F_2 and F_4.

Table 3. Angular components of the wave functions and corresponding eigenvalues of the energy of ions with d^2 and d^7 electronic configuration in weak ligand fields of symmetry C_{4v}, C_{3v} pyram, and C_{3v} tetr.

C_{4v}			$C_{3v\ pyram}$			$C_{3v\ tetr}$		
Symbol	Ψ	E	Symbol	Ψ	E	Symbol	Ψ	E
A_1	Y_3^0	$\frac{4}{5}a_2-2a_4$	A_1^-	Y_3^0	$\frac{4}{5}a_2-2a_4$	A_1^-	$\alpha' Y_3^0+\beta'\frac{(Y_3^3-Y_3^{-3})}{\sqrt{2}}$	$-\left[\frac{1}{10}a_2+\frac{3}{2}a_4+\sqrt{g}\right]$
B_1	$\frac{1}{\sqrt{2}}(Y_3^2-Y_3^{-2})$	$\frac{7}{3}a_4-b$	A_1^+	$\frac{1}{\sqrt{2}}(Y_3^3-Y_3^{-3})$	$-a_2-a_4$	A_1^+	$\beta' Y_3^0-\alpha'\frac{(Y_3^3-Y_3^{-3})}{\sqrt{2}}$	$-\left[\frac{1}{10}a_2+\frac{3}{2}a_4-\sqrt{g}\right]$
B_2	$\frac{1}{\sqrt{2}}(Y_3^2+Y_3^{-2})$	$\frac{7}{3}a_4+b$	A_2	$\frac{1}{\sqrt{2}}(Y_3^3+Y_3^{-3})$	$-a_2-a_4$	A_2	$\frac{1}{\sqrt{2}}(Y_3^3+Y_3^{-3})$	$-a_2-a_4$
E^-	$\alpha(Y_3^{-3}\pm Y_3^3)+$ $+\beta(Y_3^1\pm Y_3^{-1})$	$-\frac{1}{5}a_2-\frac{2}{3}a_4-\sqrt{h}$	E^-	$\frac{1}{\sqrt{2}}(Y_3^1\pm Y_3^{-1})$	$\frac{3}{5}a_2-\frac{1}{3}a_4$	E^-	$\alpha Y_3^{-2}-\beta Y_3^1$ $\alpha Y_3^2+\beta Y_3^{-1}$	$\frac{3}{10}a_2+a_4-\sqrt{h}$
E^+	$\beta(Y_3^{-3}\pm Y_3^3)-$ $-\alpha(Y_3^1\pm Y_3^{-1})$	$-\frac{1}{5}a_2-\frac{2}{3}a_4+\sqrt{h}$	E^+	$\frac{1}{\sqrt{2}}(Y_3^2\pm Y_3^{-2})$	$\frac{7}{3}a_4$	E^+	$\beta Y_3^{-2}+\alpha Y_3^1$ $\beta Y_3^2-\alpha Y_3^{-1}$	$\frac{3}{10}a_2+a_4+\sqrt{h}$
$a_2=\frac{1}{7}F_2(-2\xi+\eta)$; $a_4=\frac{1}{7}F_4\left(\frac{3}{2}\xi+\eta\right)$; $b=\frac{5}{6}F_4\xi$ $h=\left(\frac{1}{5}a_2+\frac{2}{3}a_4\right)^2+\frac{3}{5}b^2-(a_2+a_4)\times\left(-\frac{2}{5}a_2+\frac{1}{3}a_4\right)$.			$a_2=\frac{1}{7}F_2\left(-\frac{3}{2}\xi+\eta\right)$; $a_4=\frac{1}{7}F_4\left(\frac{9}{8}\xi+\eta\right)$.			a_2, a_4 — see Table 2 $g=\left(\frac{1}{10}a_2+\frac{3}{2}a_4\right)^2+c_{A_1}^2-\left(-\frac{4}{5}a_2+2a_4\right)(a_2+a_4)$; $h=\left(\frac{3}{10}a_2+a_4\right)^2+c_E^2+\frac{3}{7}a_4\left(-\frac{3}{5}a_2+\frac{1}{3}a_4\right)$; $c_{A_1}^2=\frac{90}{112}F_4^2\xi^2\sin^2\Delta\cos^6\Delta$; $c_E^2=\frac{10}{16}F_4^2\xi^2\sin^2\Delta\times\cos^6\Delta$.		

Since the splitting of high-spin levels which weak ligand fields induce in the $(3d)^6$ and $(3d)^4$ electronic configurations is similar to the splitting in strong ligand fields of the $(3d)^1$ and $(3d)^9$ configurations respectively, it can be discussed by reference to the results given in Table 2 and Fig. 4.[22,23]

We shall not be concerned with the behaviour of ^6S high-spin levels in weak ligand fields for $(3d)^5$ electronic configurations. The optical spectra of these ions are relatively insensitive to changes in the symmetry of the external field, and their intensity is extremely low (spin-forbidden transitions). Because of the absence of an

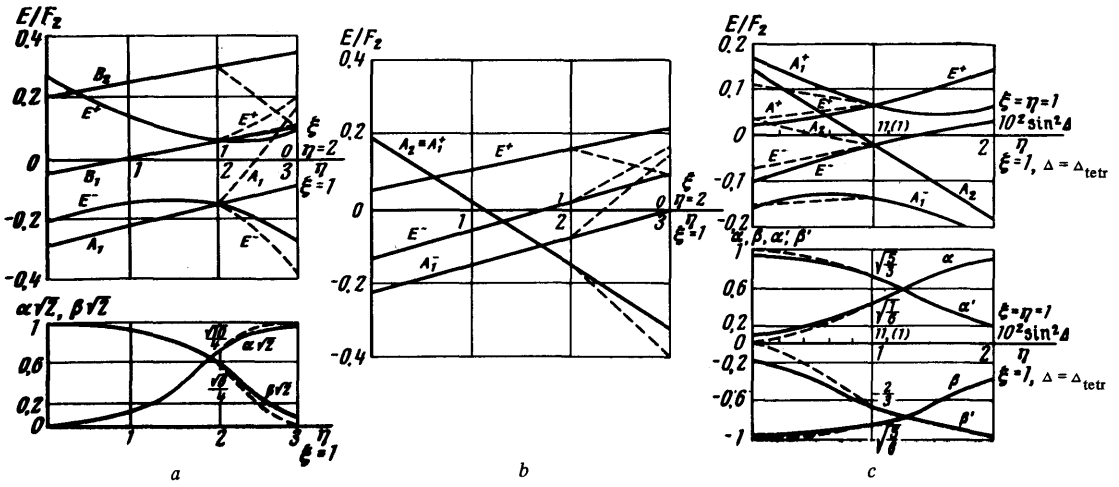


Figure 5. Splitting of the high-spin F-levels arising from the electronic configurations d^2 and d^7 in units of F_2 ($F_4/F_2 = 0.15$) in weak ligand field of symmetry (*a*) C_{4v}, (*b*) C_{3v} pyram, and (*c*) C_{3v} tetr. Figs. 5*a* and 5*b* also show plots of the coefficients in the wave functions. (The significance of the full and the broken lines is defined in the caption to Fig. 4.)

Table 4. Expressions for the spin-Hamiltonian constants of the Cu^{2+} and Co^{2+} ions in different ligand fields.

Ion	n	Ligand field symmetry	$g_\parallel$	$g_\perp$	D	Remarks
Cu^{2+}	9	C_{4v}, stretched octahedron ($\xi=1;\ \eta<2$)	$2+\frac{8\lambda}{\Delta_{B_1B_2}}$	$2+\frac{2\lambda}{\Delta_{B_1E}}$	—	$\lambda>0;\ \Delta_{ij}>0$
		C_{4v}, compressed octahedron ($\xi<1,\ \eta=2$) ($\xi=1,\ \eta>2$)	2	$2+\frac{6\lambda}{\Delta_{A_1E}}$	—	$\lambda>0;\ \Delta_{ij}>0$
		C_{3v}, compressed bipyramid ($\xi=1;\ \eta>1,4$) ($\xi=0\div1;\ \eta=1$)	2	$2+\frac{6\lambda}{\Delta_{A_1E^-}}$	—	$\lambda>0;\ \Delta_{ij}>0$
		C_{3v}, compressed tetrahedron ($\eta>1;\ \sin^2\Delta=1/9$)	2	$*2+6\lambda$	$(\alpha^2/\Delta_{A_1E^-}+\beta^2/\Delta_{A_1E^+})$	$\lambda>0;\ \Delta_{ij}>0$
		Compressed tetrahedron C_{3v}	$**g_\parallel>g_\perp>2$		$D<0$	spin ground state $\pm3/2$
		Regular tetrahedron d	$2-\frac{8\lambda}{\Delta_{A_1^-A_2}}$	$2-\frac{8\lambda}{\Delta_{A_1^-A_2}}$	$D=0$	$\lambda<0;\ \Delta_{ij}>0$
		Stretched tetrahedron C_{3v}	$**2<g_\parallel<g_\perp$		$D>0$	spin ground state $\pm1/2$
Co^{2+}	7	Trigonal pyramid C_{3v}	2	$2-12\lambda/\Delta_{A_1E}^-$	$D=\frac{6\lambda^2}{\Delta_{A_1^-E^-}}$	spin ground state $\pm1/2$ $\lambda<0;\ \Delta_{ij}>0$
		Planar triangle D_{3h}	2	$2-\frac{12\lambda}{\Delta_{A_1^-E_2^-}}$	$D=\frac{6\lambda^2}{\Delta_{A_1^-E^-}}$	spin ground state $\pm1/2$ $\lambda>0;\ \Delta_{ij}>0$

* The coefficients α and β are presented graphically in Fig. 4*c*.

** Only the analytical results are presented because the expressions are too complicated.

orbital angular momentum, the g-factor of the EPR spectrum is close to the free-electron value (*a*), and the hyperfine coupling constants are insensitive to the symmetry of the surroundings.

Table 4 lists the expressions for the spin-Hamiltonian constants of the Cu^{2+} and Co^{2+} ions in different ligand fields, needed for our subsequent discussion, and obtained from the data in Tables 2 and 3 by the method of Abragam and Pryce[26]. These expressions include the spin–orbital interaction constant (λ) of the corresponding ion and the splitting constant of its i and j electronic levels in the ligand field (Δ_{ij}).

III. RESULTS OF STUDIES ON ZEOLITES CONTAINING METAL IONS OF THE FIRST TRANSITION ROW

We shall consider the results of recent studies on zeolites containing first-row transition metal cations with a charge not greater than three, because no zeolite has yet been synthesised in which the charge of the alumina–silica lattice is compensated by cations in a still higher valency state. The results are best discussed in the order of increasing atomic number of the element introduced into the zeolite.

Scandium. The electronic configuration of the ground state of the scandium atom is $[A](3d)^1(4s)^2$, where [A] denotes the electronic structure of the argon atom. Doubly charged Sc^{2+}, with the electronic configuration $[A](3d)^1$, can be observed in principle by EPR and optical spectroscopy, but there are no references in the literature to zeolites containing bivalent scandium ions. A zeolite of type Y containing tervalent scandium ions with the [A] electronic configuration has been investigated[27] as a cumene cracking catalyst. In the same work it was shown by X-ray diffraction that extensive exchange of Na^+ ions by Sc^{3+} ions tends to disrupt the zeolite lattice.

Titanium. The electronic configuration of the ground state of the free titanium atom is $[A](3d)^2(4s)^2$. No work on zeolites containing Ti^{2+} or Ti^{3+} ions has come to our notice, probably because of the difficulty of preparing these zeolite forms.

Vanadium. The electronic configuration of the ground state of the free vanadium atom is $[A](3d)^3(4s)^2$.

Vanadium has been introduced into zeolites only as the doubly charged vanadyl cation $[VO]^{2+}$. The EPR spectra of these zeolites are reported[28] to be identical to the EPR spectrum of vanadyl in solution. No other information concerning the behaviour of vanadyl in the zeolite lattice is available. A strong internal ligand field is known to exist in the vanadyl ion: this field is mainly responsible for the optical and paramagnetic properties of the ion. The spectral parameters of the vanadyl ion are relatively insensitive to the coordination of the cation, and therefore a detailed description of the behaviour of vanadyl in zeolites cannot be expected from EPR and optical spectral studies. This conclusion, however, is not indisputable.

Zeolites containing vanadium ions in other valency states have not been prepared or investigated. An optical study of zeolites containing V^{3+} cations would be very interesting.

Chromium. The electronic configuration of the ground state of the free chromium atom is $[A](3d)^5(4s)^1$. Only zeolites containing tervalent chromium ions have so far been prepared.

We shall consider the effects which can be expected in the optical spectra of zeolites containing Cr^{3+} ions.

The spectrum of the octahedral $[Cr(H_2O)_6]^{3+}$ complex has been discussed fully[29]. The splitting diagram of the ^4F level of the ground state of the free Cr^{3+} ion in fields of C_{4v} symmetry (distorted along the four-fold octahedral axis) is shown in Fig. 5*a* with the sign of the vertical axis reversed. The optical spectra of aqueous solutions of tervalent chromium salts reveal two optical transitions within the ^4F level ($^4A_2 \rightarrow {}^4T_1$; $^4A_2 \rightarrow {}^4T_2$). It is evident from Fig. 5*a* that for a ligand field corresponding to an octahedron stretched along its four-fold axis (case of $\eta < 2$, $\xi = 1$) the absorption bands of the optical spectrum should split into two, the transitions $B_2 \rightarrow B_1$ and $B_2 \rightarrow A_1$ remaining approximately in the original positions and the transitions $B_2 \rightarrow E^-$ and $B_2 \rightarrow E^+$ undergoing a shift towards the red end of the spectrum. If the absorption bands are sufficiently broad, this effect manifests itself as a broadening of the bands accompanied by a displacement of their centre of gravity towards longer wavelengths. The same shift, but without band broadening, is produced by a weakening of the ligand field whilst retaining the octahedral symmetry.

If the octahedron surrounding the ion is compressed along its four-fold axis, the absorption bands of the Cr^{3+} ions are again broadened, but the shift is towards the blue end of the spectrum.

The optical reflectance spectra in diffuse scattered light of A, X, and Y zeolites containing tervalent chromium ions have been investigated by the present writers together with Minachev and others[30]. Since all the spectra (after cation exchange) consisted of three absorption maxima at 285, 425, and 625 nm, i.e. in the same positions as those in the optical spectra of Cr^{3+} solutions, it was concluded that the chromium ions exist as hexaquo complexes $[Cr(H_2O)_6]^{3+}$ in the zeolite structure. After vacuum heat treatment at 200–250° the samples lost most of the adsorbed water, and the absorption bands of the optical spectrum became broader and were shifted towards the red. This effect was explained by assuming that the ligand field had been weakened by the removal of the water from the second coordination sphere of the chromium ion. It follows from the above discussion that the replacement of one water molecule in the first coordination sphere of the Cr^{3+} ion by a weaker ligand (e.g. oxygen from the zeolite lattice) should lead to the same result. Both the two proposed band-broadening and band-shift mechanisms probably operate in the present system.

In zeolites of types A and X these changes in the optical spectrum were found to be irreversible, since the original spectrum of the hexaquo complex could not be reproduced by hydrating the samples at room temperature. This effect was ascribed to incipient breakdown of the zeolite lattice of CrNaX and CrNaA upon vacuum heat treatment at temperatures above 200°, which had been demonstrated independently by differential thermal analysis and thermovolumetric analysis. In contrast, with CrNaY zeolite (known to be stable up to 700°) the reflectance spectrum after water adsorption at room temperature was found to be practically identical to the spectrum recorded on the initial sample after cation exchange.

After vacuum heat treatment at 400° the optical spectrum of CrNaY zeolite showed some radical changes: the sample developed a grey colour and began to absorb over practically the whole of the visible region of the spectrum, suggesting complete breakdown of the hydration shell of the Cr^{3+} ions. The spectral changes were irreversible towards water adsorption, despite the evidence (from differential thermal and thermovolumetric analyses) that the zeolite crystal structure had survived the heat treatment. This observation was interpreted by assuming that the dehydrated Cr^{3+} ions at high temperatures can penetrate within the sodalite cells, where they experience a ligand field with a lower symmetry (probably on *SI′* sites). These holes are too small to accommodate the hexaquochromium complexes, and therefore the optical spectra after exposure to water do not revert to their original form (though some minor changes can be seen). This interpretation, which is consistent with the demonstration[31] by X-ray diffraction analysis that tervalent lanthanum cations penetrate into the small holes of LaNaY zeolite after dehydration, was further confirmed by studies of the adsorption of ethanol and diethyl ether.

Tsitsishvili and Urushadze[32] have reported an EPR study of magnetically concentrated samples of CrNaA zeolite. They observed the EPR spectra of samples, both hydrated and vacuum-dehydrated at room temperature, and found in every case a single broad line (up to 500 G) with a g-factor close to 2, which they ascribed to the octahedral hexaquocomplex $[Cr(H_2O)_6]^{3+}$. After dehydration at room temperature the lines became slightly broader.

Chromium-containing zeolites dehydrated at higher temperatures have not been studied by EPR, because the thermally stable CrNaY zeolites tend to contain iron impurities which give a broad and strong EPR signal[33], and interfere with the study of other paramagnetic ions with broad signals‡.

Before examining in detail the results of EPR measurements, we shall consider some effects which may be present in the EPR spectra of Cr^{3+} ions localised in *SI′* sites. As stated above, the ligand field in this case has the symmetry of a tetrahedron distorted along a trigonal axis. It is evident from Fig. 5*c* that the ground state of a Cr^{3+} ion in a tetrahedron extended along a trigonal axis is not orbitally degenerate, and could give rise to an EPR

‡ A sample of CrNaY zeolite in which 27% of the Na^+ had been exchanged by Cr^{3+}, and which gave no EPR signal in its sodium form, was kindly provided for our EPR measurements by No. 20 Laboratory of the Institute of Organic Chemistry of the USSR Academy of Sciences (Kh. M. Minachev's Industrial Laboratory).

signal at low enough temperatures. An analogous situation involving the Cr^{3+} ion was reported by Henning and coworkers [34]. In a tetrahedron compressed along the trigonal axis the ground state of the Cr^{3+} ion is doubly orbitally degenerate, and the spin–orbital interaction λLS splits it into four doublets which are described by the following wave functions (including the spin variables):

E (energy)	Ψ
$9/4\,\lambda$	$\Psi_1\chi(-3/2)$; $\Psi_2\chi(3/2)$;
$3/4\,\lambda$	$\Psi_1\chi(-1/2)$; $\Psi_2\chi(1/2)$;
$-3/4\,\lambda$	$\Psi_1\chi(1/2)$; $\Psi_2\chi(-1/2)$;
$-9/4\,\lambda$	$\Psi_1\chi(3/2)$; $\Psi_2\chi(-3/2)$;

$$\Psi_1 = -\sqrt{\frac{5}{6}}Y_3^{-2} + \sqrt{\frac{1}{6}}Y_3^1; \qquad \Psi_2 = -\sqrt{\frac{5}{6}}Y_3^2 - \sqrt{\frac{1}{6}}Y_3^{-1};$$

where $\chi(m)$ is the spin wave function for the spin $S = 3/2$ with a projection m on the z axis.

It can easily be shown that none of these doublets can give an EPR signal.

We have shown experimentally [35] that the EPR spectra of CrNaY samples measured at 4.2, 77, and 300°K become gradually weaker as the dehydration temperature is increased, and are practically undetectable after vacuum dehydration above 450°. This confirms our earlier conclusion [30] that after dehydration the Cr^{3+} ions penetrate into small holes and become localised at *SI'* sites. It may be argued that one water molecule (or its fragments O^{2-} or OH^-) is retained in the coordination sphere of the Cr^{3+} ion after heat treatment, and gives rise to the observed compression of the tetrahedron along its trigonal axis. This suggestion is consistent with the conclusion [31] that cation pairs of the type $M^{3+}_{SI'}...O^{2-}...M^{3+}_{SI'}$ are formed.

An effect of the zeolite crystal structure on the mechanism of cation exchange has also been reported [30]. By comparing the amount of chromium introduced into zeolites of different types under otherwise identical conditions with the amount of exchangeable sodium ions it was concluded that exchange in type A zeolites occurs only in the near-surface regions of the microcrystallites. (It should be noted that the hexaquo complexes are larger than the diameter of the windows leading into the structural pores of this type of zeolite.) Exchange does not proceed to completion even in type X zeolites, suggesting partial blocking of the windows leading into the large holes by the hexaquo complexes in the *SIII* position. This blocking effect does not take place in type Y zeolites, evidently because only a small fraction of the exchangeable Na^+ ions is in the *SIII* position (see Table 1).

Manganese. The electronic configuration of the ground state of the free manganese atom is $[A](3d)^5(4s)^2$. Only Mn^{2+} ions have been introduced into zeolites by cation exchange. The optical spectra of bivalent manganese have a very low intensity, because the transitions are spin-forbidden: this may be the reason for the lack of publications describing optical investigations of manganese zeolites.

On the other hand, a considerable volume of work on these zeolites using EPR has been published. The reason may be that in weak ligand fields the ^6S level of the Mn^{2+} ion has no closely spaced excited states, and therefore the EPR signals can be observed over a wide range of temperature and of ligand field symmetry. The experimental results are interpreted, on the whole, with the help of the theoretical concepts developed by Bleaney and Rubins [36–38]. However, the spectra of polycrystalline samples are very difficult to interpret: although the EPR spectra of Mn^{2+} ions retain their fine structure in weakly distorted octahedral and tetrahedral ligand fields, powders usually show only the ±1/2 transition because the strong angular dependence of the lines corresponding to the residual transitions give rise to fine structure. At low D values ($D/g\beta H \ll 1$), typical of the Mn^{2+} ion, the position of the lines corresponding to this transition is insensitive to the symmetry of the ligand field, and only the shape and width of some of the components of the hyperfine structure are affected (as a result of second-order effects) by changes in the surroundings of the ion. However, the hyperfine parameters, which are easily observed for the Mn^{2+} ion, are determined essentially by the degree of covalency of the bonds between the central ion and the ligands, and to a much lesser extent by the symmetry of the surroundings.

The first attempt to investigate zeolites of types X and Y containing Mn^{2+} ions by the EPR method was made by Ursu and Nicula [39] in 1964. These workers found that the resolution of the hyperfine structure of EPR spectra measured at 9 300 MHz depended on the high-temperature dehydration treatment to which the sample had been exposed. The effect was ascribed to changes in ligand-field symmetry arising from the removal of water molecules, but no attempt was made to propose a concrete model of the location of the ions in the zeolite structure.

The next series of publications, also involving EPR measurements at 9 300 MHz, was due to Barry and Lay [33,40,41]. These workers studied zeolites of types X and Y containing manganese ions in combination with the diamagnetic ions Li^+, Na^+, K^+, Cs^+, Mg^{2+}, Ca^{2+}, Zn^{2+}, and La^{3+}. Using the Mn^{2+} ions as a "paramagnetic probe", they tried to explain some features of the distribution, in zeolites, of cations devoid of paramagnetism.

The complex and poorly resolved experimental spectra, varying with sample treatment, were ascribed to Mn^{2+} ions in different states, giving rise to their individual spectra with the following parameters:

A: $g = 2.000$; $A = 97 \pm 3.5$ G;
I: $g = 2.001$; $A = 95 \pm 1.5$ G; $D = 54 \pm 18$ G;
II: $g = 2.001$; $A = 95 \pm 1.5$ G; $D = 131 \pm 3.5$ G (occasionally $D = 100$ G);
(i): $g = 1.996$; $A = 76.5 \pm 2$ G; $D = 65 \pm 35$ G
(ii): $g = 1.995$; $A = 88.5 \pm 3$G; $D < 130$G.

The states were assigned by the authors as follows: A—hydrated $(Mn \cdot nH_2O)^{2+}$ ions; I—Mn^{2+} ions localised on *SI* sites; II—Mn^{2+} ions localised on *SI'*, *SII'*, or *SII* sites; (i), (ii)—Mn^{2+} ions localised on *SI'* sites with a strong covalent bond to hydroxyl (OH^-) or O^{2-} ions respectively.

However, none of the spectra (with the exception of the hydrated sample) was observed in a pure form, and the spectral assignments to manganese ions in different lattice positions are not entirely convincing because they are not supported by serious arguments based on the structure of the paramagnetic centres. For example, the observed D values vary between 0.50×10^{-2} and 1.3×10^{-2} cm^{-1} and therefore correspond to a weakly distorted cubic field: they can hardly be quoted as evidence for any particular mode of stabilisation of the Mn^{2+} ion. The hyperfine coupling constants also did not vary over a wide range, with the exception of spectrum (i), ascribed to tetrahedral Mn^{2+} ions containing a hydroxyl group in the coordination sphere. Lastly, Barry and Lay's interpretation was not confirmed by the more recent work of Tikhomirova and coworkers [42] at a frequency of 35 000 MHz.

Because of the EPR spectrum of Mn^{2+} ions in a low-symmetry ligand field is greatly complicated by second-order effects, resulting in overlap of the hyperfine components and in the appearance of nuclear-spin-forbidden transitions, these workers carried out their measurements in an apparatus working at a shorter wave-length. They showed[42] that by working at a higher frequency ($\lambda \simeq 8$ mm, $\nu \simeq 37\,500$ MHz) the EPR spectra of Mn^{2+} ions in hydrated MnNaA, MnNaX, and MnNaY zeolites become much simpler and consist of well resolved sextets. From the intensity ratios of forbidden and allowed transitions they obtained a D value close to 106 G. They subsequently published a more detailed study of the behaviour of Mn^{2+} ions in the sodium forms of A, X, and Y zeolites during dehydration and adsorption of water vapour[43,44]. However, their conclusions rely exclusively on changes in the hyperfine coupling constants of the EPR spectra.

Since the EPR spectra of the Mn^{2+} ions in the initial samples of A, X, and Y zeolites have parameters almost identical to those of the EPR spectra of aqueous solutions ($A = 96$ G), the authors assume that the Mn^{2+} ions in this case are present in the form of aquo complexes. Dehydration at temperatures up to 150° gives EPR spectra with a hyperfine splitting constant of 87 G for all types of zeolite, which is ascribed to partially dehydrated Mn^{2+} ions. It is also pointed out that the electronic state of partially dehydrated Mn^{2+} ions is unaffected by the charge on the zeolite lattice or by the geometry of its framework.

If the dehydration temperature is raised above 150°, three types of spectrum are observed in X and Y zeolites ($A = 99$ G, $g = 2.000$; $A = 87$ G, $g = 2.000$; $A = 87$ G, $g = 2.007$), and two types of spectrum in type A zeolite ($A = 87$ G, $g = 2.000$; $A = 73$ G, $g = 2.000$). After dehydration at 300–400°, X and Y zeolites give only one EPR signal ($A = 99$ G, $g = 2.000$), and the spectra of type-A zeolites remain practically unchanged. The authors point out that the total intensity of all the spectra for a given sample remains constant.

By analogy with the interpretation of the spectra of Mn^{2+} ions in spinels[45], it is suggested that the EPR signal in a type-A zeolite with a hyperfine splitting of 73 G arises from ions localised in the neighbourhood of a six-membered oxygen ring and on the side of a small hole (site *SII'*, see Fig. 2), within which a residual water molecule is assumed to remain even after high-temperature vacuum treatment. In this case, the Mn^{2+} ion is tetrahedrally surrounded by oxygen atoms from the lattice (at 3 corners) and water (at 1 corner). This interpretation, with the Mn^{2+} ion in an *SII'* site rather than an *SII* site, is supported by the observation that water vapour adsorption must be carried out at a relatively high temperature (~ 80°) in order to reproduce the EPR spectrum with a splitting of 87 G characteristic of the partially hydrated Mn^{2+} ion.

The EPR spectra of fully dehydrated X and Y zeolites, with a hyperfine splitting of 99 G, are assigned to Mn^{2+} ions in *SI* sites, where the ligand field is octahedral. An alternative explanation is also discussed: localisation of Mn^{2+} within a small zeolite hole, since the adsorption of water and ammonia vapour gradually yields EPR spectra corresponding to the fully hydrated initial samples.

No attempt was made to interpret the EPR spectrum of Mn^{2+} ions with a splitting of 87 G and a g-factor of 2.007.

The results obtained for MnNaY zeolites by Barry and Lay are compared with those of Tikhomirova and coworkers in Table 5. Except for the data relating to the initial samples, substantial differences in experimental results and in their interpretation are evident. The discrepancy is due partly to differences in dehydration conditions, and partly to incorrect treatment of the results obtained at 9 300 MHz from poorly resolved spectra. However, the remaining doubt will not be fully removed until EPR measurements are carried out at both radio frequencies simultaneously, under standard conditions of heat treatment and with standard control of the residual water.

It may be concluded from the above review of published EPR work on synthetic zeolites containing bivalent manganese ions that the existence of Mn^{2+} in various states within the zeolite structure has been proved beyond doubt. However, because of the spectroscopic peculiarities of this ion, the detailed interpretation of the results is still tentative.

Table 5. Results obtained by different workers for type-Y zeolites containing Mn^{2+} ions.

	Initial	Partly dehydrated	Fully hydrated	References
Hyperfine splitting constant, A	96 G	99 G 87 G 87 G	99 G	42—44
Interpretation	$[Mn(H_2O)_6]^{2+}$, large hole *SIII*	*SII*, *SI*? $(Mn \cdot n H_2O)^{2+}$ not interpreted	*SII*, *SI*?	
Hyperfine splitting constant, A	97 G	95 G, 76 G	95 G	33,40,41
Interpretation	$(Mn \cdot n H_2O)^{2+}$	*SII*, *SI'* $[MnOH]^+$ *SII'*?	*SI'*, *SII*, *SII'*?	

Iron. The electronic configuration of the ground state of the free iron atom is $[A](3d)^6(4s)^2$. Tervalent iron ions can give rise to EPR spectra. However, we have been unable to find any reference to structural studies of zeolites containing ferric ions by EPR or by optical spectroscopy. Such zeolites have been synthesised, and are being intensively studied by gamma-resonance spectroscopy[46–50]. The main results, formulated by Delgass and coworkers[50], indicate that the Fe^{2+} cations in dehydrated type-Y zeolite are in a high-spin state, and occupy two types of site: *SI* (inaccessible to adsorbed molecules) and *SII* (accessible to adsorbed molecules). It is shown[44] that zeolites of types X and A are broken down by the introduction of iron ions.

The absence of EPR studies is probably due to the complexity of the EPR spectra of Fe^{2+} and Fe^{3+} ions in surroundings of low symmetry, making interpretation impossible without a special theoretical study. Not the least of the difficulties is the presence of iron impurities in the sodium forms of zeolites even before exchange, already mentioned above, which complicates the application of EPR to these systems[33]. It should not be concluded, however, that the EPR method will not be used in future to study zeolites containing iron ions.

Difficulties may arise also in the interpretation of the optical spectra of zeolites containing Fe^{3+} ions. Having an electronic structure similar to that of the Mn^{2+} ion, the Fe^{3+} ion gives strong charge-transfer bands in the near u.v. region (see Ref. 51, p. 276), with fairly strong "shoulders" in the visible region of the spectrum which tend to mask the weak, spin-forbidden d–d transitions. Optical studies of zeolites containing Fe^{2+} $(3d)^6$ ions could give very interesting results, but the d–d transitions for

the high-spin Fe^{2+} ion lie in the near i.r. region: the $^5T_{2g} \rightarrow {}^5E_g$ transition for the hexaquo Fe^{2+} ion is observed at ~ 10000 cm^{-1} (p. 271 of Ref. 51).

Cobalt. The electronic configuration of the ground state of the free cobalt atom is $[A](3d)^7(4s)^2$. Only zeolites containing bivalent cobalt ions have so far been synthesised and investigated.

There are many references in the literature to the splitting of the energy levels of the bivalent cobalt ion, and to its magnetic properties, in the weak ligand fields corresponding to a distorted octahedron (see, for example, Ref. 52). We shall therefore confine this review to a qualitative discussion of the optical and magnetic properties of the Co^{2+} ion in weak ligand fields of symmetry C_{3v} and C_{3v} tetr. In these cases the ground state of the Co^{2+} ion ($S = 3/2$) is described by a wave function with an angular component which gives rise to an irreducible representation A_1 of the group C_{3v} (see Table 3 and Figs. 5*b* and 5*c*). Since the transitions between the levels of the split ^4F level lie in the i.r. region and are relatively weak, only the strong transition to the excited ^4P level is usually observed in the optical spectrum (see, for example, Ref. 51). Changes in ligand-field symmetry from a tetrahedron compressed along the trigonal axis to an extended tetrahedron, a trigonal pyramid, of a planar triangle should not significantly affect the spectral position of this optical transition, since the main contribution to its energy comes from the energy difference between the ground ^4F level and the excited ^4P level of the free Co^{2+} ion.

However, fairly substantial changes in the EPR spectra can be expected to result from these changes in ligand field. Table 4 shows the results of an analysis of the expressions for the g and D tensors of the Co^{2+} ion in fields of T_d, C_{3v} tetr, C_{3v} pyram, and D_{3h} symmetry, and also lists the spin ground states in a zero magnetic field.

In a tetrahedron compressed along the trigonal axis the constant D for this interaction is negative for the Co^{2+} ion (see Table 4). Since the EPR signals of Co^{2+} are usually observed at $T = 4.2°K$ ($kT \simeq 3$ cm^{-1}) because of the short relaxation times, the population of the $\pm 1/2$ spin doublet, which gives rise to the EPR signal, can be very small for $D < 0$ and $|D| \gg kT$. Hence it is obvious that the EPR signals of polycrystalline samples are difficult to observe when the surroundings of the Co^{2+} ion correspond to a tetrahedron highly compressed along the trigonal axis ($D < 0$). For example, Owen and Bowers[53] find $D = -4.5$ cm^{-1}, so that the population of the $s = \pm 1/2$ spin doublet is only $-2|D|/ekT \simeq 0.05$. Little gain in the intensity of the EPR signal can be expected from carrying out the measurement at liquid-nitrogen temperature, because the 10-fold increase in the population of the $\pm 1/2$ doublet (to 0.5) is compensated by a decrease in the difference of the populations within the doublet by a factor of $77°/2.4° = 18$. Line broadening may also appear as a result of relaxation.

On changing from compression to extension of the tetrahedron along the trigonal axis the hyperfine interaction constant changes sign, and remains positive throughout further changes in the coordination of the ion (up to the coordination of a planar triangle). Under these conditions the population of the $\pm 1/2$ spin doublet is close to 1: evidently, this should lead to a sharp increase in the strength of the EPR signal as compared with the case discussed above.

It follows that differences in the relative intensity of the EPR spectra of Co^{2+} ions in different samples can be used as a criterion of the presence of distortions in the tetrahedral ligand field, which (as stated above) do not materially affect the optical properties.

The position of the components of the fine structure of EPR spectra for a spin of 3/2 and $|D| \gg g\beta H$ has been fully discussed[54].

The most significant structural data on cobalt-containing zeolites, published up to 1970, were obtained by optical reflectance spectroscopy in the visible and near u.v. regions of the spectrum.

It has been shown[55] that the adsorption of substances such as H_2O, NH_3, CH_3OH, etc. on dehydrated CoNaA zeolites is accompanied by a colour change, which suggests that molecules of these compounds can enter the coordination sphere of Co^{2+} ions.

A recent paper by Klier[56] shows, on the basis of optical data, that the Co^{2+} ion in dehydrated type-A zeolite is localised in the plane of the six-membered oxygen window, whereas after adsorption of N_2O molecules its coordination increases to the tetrahedral configuration. Klier stresses the reversibility of this process upon outgassing the sample at 50°, but at 150° the nitrous oxide decomposes catalytically into molecular nitrogen and oxygen.

Barry and Lay[41] observed, in their study by reflection spectroscopy of CoNa13X zeolite dehydrated at 300°, that the Co^{2+} ions are located in a tetrahedral ligand field. Hence they suggested that the ions are localised in *SI'* sites in this zeolite. Three of the planar ligands are lattice oxygen atoms, and the fourth ligand is a residual water fragment (OH^- or O^{2-}). It is not clear, however, why *SI'* sites are chosen in preference to *SII'* or *SII* sites, since measurements of the specific adsorption of nitrous oxide[40] have shown that the Co^{2+} ions can be localised also in sites accessible to the molecules of adsorbate.

Until recently there were no published references to EPR studies of cobalt-containing zeolites, evidently because of the need to work at liquid-helium temperatures. We have recently reported[57] an investigation of this type on X and Y zeolites, carried out in cooperation with Brotikovskii. Since no significant difference could be found between the spectra (either optical, or ESR) of these two types, we shall confine the following discussion to the results obtained for the zeolite of type Y.

EPR and optical spectra were recorded before and after dehydration by vacuum baking. (The dehydration–rehydration cycle was found to be fully reversible.) The spectra were practically identical to those of aqueous solutions of Co^{2+} salts, suggesting that the cobalt ions after exchange (and rehydration) exist as $[Co(H_2O)_6]^{2+}$ aquo-complexes, located in large zeolite holes.

Vacuum baking at 100° removes only some of the water from the zeolite, and the Co^{2+} ions retain their hexaquo coordination. This is confirmed by the optical reflectance spectra, in which the absorption bands are only slightly displaced towards the red (from 19000 to 17000 cm^{-1}), with a somewhat increased intensity, after vacuum baking.

Dehydration at 200–500° produces a blue colour in the samples, characteristic of the tetrahedral compounds of bivalent cobalt, and strong, overlapping bands appear in the optical spectra at 18500, 17000, and 15100 cm^{-1}. Since, as already stated, the position of these bands is relatively insensitive to distortions of the tetrahedral surroundings of Co^{2+}, it is not easy to assign the localisation of the cobalt ions to *SI'*, *SII'*, or *SII* sites.

On the other hand, we can deduce from the EPR spectra of samples dehydrated at 200–500° that after this treatment the Co^{2+} ions exist in two different states within the zeolite. For dehydration temperatures of 200–350° they

lie on SII sites, with the coordination of a tetrahedron compressed along its trigonal axis. The fourth (axial) ligand is assumed to consist of residual water molecules or water fragments (OH^- or O^{2-}). As stated above, polycrystalline samples may fail to give an EPR signal under these conditions because the ±1/2 spin doublet is lightly populated ($D < 0$). The EPR signal disappears completely[57], and reappears ($g_\parallel \simeq 2.00$; $g_\perp \simeq 2.75$) only after heating the sample at higher temperatures (400–500°). We have ascribed the spectra observed under these conditions to Co^{2+} ions localised in the plane of the six-membered oxygen window (between SII′ and SII sites). As Table 4 shows, $g_\parallel$ should be approximately 2 in this case, and $g_\perp > 2$, as observed experimentally. We have not considered the possibility of localisation of Co^{2+} ions in SI′ sites, because the adsorption of tertiary pentanol molecules on a dehydrated sample is known to alter the EPR spectrum, suggesting that quite large molecules can enter the coordination sphere of the Co^{2+} ion.

Summing up all that has been said on zeolites containing Co^{2+} ions, we stress that these cations can be introduced by exchange into zeolites of type X and Y in the form of octahedral aquo-complexes $[Co(H_2O)_6]^{2+}$, which "float" in the large holes of the zeolite lattice. As the samples are dehydrated, the cobalt ions are transferred initially to SII sites, where they retain a water molecule or fragment (OH^- or O^{2-}) in the first coordination sphere, and finally to the six-membered windows of the sodalite cells, where they remain accessible to adsorption of various molecules.

In conclusion, we note that Co^{2+} ions can be reduced if the host zeolite is dehydrated under reducing conditions. Thus, reproducible results on water adsorption at room temperature can be obtained only if the sample is carefully protected from the vapours of vacuum grease and other organic materials[57].

Nickel. The electronic configuration of the ground state of the free nickel atom is $[A](3d)^8(4s)^2$. One of the first papers describing optical and EPR studies of nickel-containing X and Y zeolites is due to Rabo and coworkers[58], who used EPR to observe the Ni^{1+} ion (electronic structure $[A](3d)^9$), obtained by reducing the samples in alkali metal vapours or in hydrogen, and also the signal from ferromagnetic metallic nickel. On the assumption that reduction of the ions does not cause them to migrate to new sites, the authors conclude that for 5–75% exchange of Na^+ by Ni^{2+} ions in dehydrated X and Y zeolites the ions occupy SII as well as SI sites. The EPR spectrum with $g_\parallel = 2.30 + 2.40$ and $g_\perp = 2.096$ is ascribed to Ni^{1+} cations localised in SI sites, and the spectrum with $g_\parallel = 2.10 + 2.13$ and $g_\perp = 2.065$ to Ni^{1+} in SII sites. Optical data were used to give a theoretical interpretation of the g-tensor values obtained from the EPR spectra. A wide absorption band at 450 nm was ascribed to Ni^{2+} ions in SII sites, and a band at 650 nm ($^2E_g \rightarrow {}^2T_g$ transition) was ascribed to Ni^{1+} ions in SII sites. The spin–orbital interaction constant found by comparing EPR and optical results was 500 cm^{-1}, in good agreement with the value for the free Ni^{1+} ion ($\lambda = 600$ cm^{-1}).

Adsorption experiments with oxygen, carbon monoxide, hydrogen, and ammonia on reduced forms of nickel zeolite have shown that Ni^{1+} ions localised on SII sites interact most strongly with adsorbed molecules, but at high temperatures the Ni^{1+} ions on SI sites also take part in the reaction $Ni^{1+} + O_2 \rightarrow Ni^{2+} + O_2^-$ during oxygen adsorption.

Olson[59] was able to confirm these conclusions by X-ray diffraction methods in his study of natural faujasite containing nickel ions ($SiO_2/Al_2O_3 = 4.6$). He found the following distribution of Ni^{2+} ions in the elementary cell of the mineral:

Site	SI	SI′	SII′	SII	SI′ + water fragment	SII′ + water fragment
Amount	10.5	3.2	2.0	6.5	5.8	2.9

From these data it was concluded that the results of X-ray diffraction analyses of zeolites in their calcium form cannot be applied automatically to zeolites containing transition-metal ions. Thus, whereas the preferred sites for alkaline-earth cations in the zeolite structure are the SI sites[60,61], and the preferred sites for rare-earth cations are the SI′ sites[31], transition-metal cations can be localised in other sites of the zeolite lattice even at low extents of exchange.

Detailed optical studies of type-A zeolite containing bivalent nickel ions have been reported by Polák and Černý[62] and Klier and Ralek[63]. The former have made computer calculations, using ligand-field theory, of the electronic spectra of ions with the $(3d)^{2,8}$ electronic configuration in a crystal field with D_{3h} symmetry. The latter workers used these theoretical calculations to analyse the diffuse reflectance spectra of NiNaA zeolites degassed at different temperatures.

They showed that in a fully hydrated zeolite the bivalent nickel ions are present as the $[Ni(H_2O)_6]^{2+}$ hexaquo complex, as shown by the almost exact correspondence of their spectra with those of aqueous solutions of nickel salts.

In partly dehydrated zeolites the Ni^{2+} ions retain approximately one molecule of water in their first coordination sphere, and they become firmly bonded to the zeolite lattice—probably in SII sites—thereby acquiring distorted tetrahedral surroundings. However, the observed optical spectra did not show the characteristic absorption maxima of tetrahedral nickel at 600–700 nm (see Ref. 51, p. 301). Further dehydration causes complete removal of the water, and the Ni^{2+} cations become localised in the plane of the six-membered oxygen window of the zeolite lattice, as shown by the good agreement between the observed and the theoretically calculated optical spectrum.

Studies were made also of the adsorption of nitric oxide, cyclopropane, ethylene, propene, and acetylene on dehydrated zeolite, and it was concluded that the process is monocentric and (with the exception of acetylene) reversible. It is assumed that the nickel cation completes its coordination sphere in the form of a trigonally distorted tetrahedron.

It has been shown by X-ray diffraction analysis[64] and by magnetostatic and ferromagnetic resonance methods[65] that Ni^{2+} ions are reduced to metallic nickel by treatment of the zeolite in a reducing atmosphere, forming microcrystals approximately 100 Å in size on the surface of zeolite single crystals.

Copper. The electronic configuration of the ground state of the free copper atom is $[A](3d)^9(4s)^2$. Many papers have been written on EPR studies of zeolites containing bivalent copper cations. Cu^{2+} ions, having the $(3d)^9$ electronic configuration (nuclear spin 3/2), give very sharp EPR spectra in magnetically dilute systems: the parameters of these spectra depend sensitively on the symmetry of the immediate surroundings of the ion. The isotropic and anisotropic hyperfine interaction constants, g-tensor components, and temperature dependence of the spectrum can often be used to determine not only the coordination of the Cu^{2+} ion, but also the percentage

covalency of the bond in the complex, and also the type of motion of the complex as a whole. Hence, zeolites containing Cu^{2+} ions are specially interesting to research workers.

We shall first of all consider some optical and magnetic properties of the Cu^{2+} ion in ligand fields with C_{3v}, C_{4v}, and D_{3h} symmetry in the light of the above calculations.

As Fig. 4*a* shows, the ground state of the Cu^{2+} ion in ligand fields with O_h symmetry is doubly degenerate, and therefore the three possible d–d transitions in the optical spectra merge into one. When the octahedron is stretched along the tetrad axis we expect (see Fig. 4*a*, $\eta < 2$, $\xi = 1$) the observed absorption band to split into two, one band remaining in its original position ($B_1 \rightarrow B_2$) and two other bands appearing at shorter wavelengths ($B_1 \rightarrow E$). In a compressed octahedron, as shown in Fig. 4*a*, the splitting of the absorption band is accompanied by a shift of all three maxima towards the short-wave end of the spectrum.

We shall now turn to the changes in the EPR spectra arising from these distortions. Octahedral complexes of Cu^{2+} ions, when subjected to a weak tetragonal distortion corresponding to stretching of the octahedron, are known to give EPR spectra whose parameters are described by the expressions

$$g_{\parallel} = 2 + \frac{8\lambda}{\Delta_{B_1B_2}}; \quad g_{\perp} = 2 + \frac{2\lambda}{\Delta_{B_1E}} \quad (\text{where: } \lambda > 0,\ \Delta_{ij} > 0).$$

Obviously, in a weakly stretched octahedron $\Delta_{B_1B_2} \simeq \Delta_{B_1E}$, and therefore $\Delta g_{\parallel}/\Delta g_{\perp} \simeq 4$. As Fig. 4*a* shows, the transition from a weakly stretched octahedron to a square pyramid or to a square plane does not affect $\Delta_{B_1B_2}$, but since Δ_{B_1E} increases, the ratio $\Delta g_{\parallel}/\Delta g_{\perp}$ must also increase.

Transition from an octahedron stretched along the tetrad axis to a compressed octahedron leads to the following expressions for the components of the g-factor: $g_{\parallel} = 2$; $g_{\perp} = 2 + 6\lambda/\Delta_{A_1E}$, and therefore the EPR spectrum should become inverted, since the perpendicular component of the spectrum now finds itself at a smaller field than the parallel component.

It is evident from Fig. 4*b* and 4*c* that the ground state of the Cu^{2+} ion is not orbitally degenerate in a compressed trigonal bipyramid or in a tetrahedron compressed along the trigonal axis (the expressions for the g-factors are given in Table 4).

We should stress that in this case, as in the case of a field with the symmetry of a compressed octahedron, the perpendicular component of the EPR spectrum experiences weaker fields ($g_{\perp} > 2$) than the parallel component ($g_{\parallel} = 2$). This is because the electronic ground level in both cases is described by a wave function with an angular component Y_2^0.

In fields with the symmetry of a stretched pyramid or of a tetrahedron stretched along the trigonal axis the ground level of the Cu^{2+} ion becomes doubly orbitally degenerate (see Figs. 4*b* and 4*c*). The angular parts of the wave functions corresponding to this doublet can be written in the following general form (see Table 4):

$$\psi_1 = \alpha Y_2^2 - \beta Y_2^{-1},$$

$$\psi_2 = \alpha Y_2^{-2} + \beta Y_2^1, \text{where: } 1 \leqslant \alpha < \sqrt{\frac{2}{3}},\ \alpha^2 + \beta^2 = 1.$$

The spin-Hamiltonian which describes the behaviour of the system allowing for spin–orbital interaction and interaction with a magnetic field can be written

$$\mathcal{H} = \lambda \mathbf{LS} + \beta(\mathbf{L} + 2\mathbf{S})\mathbf{H}, \quad S = {}^1/_2.$$

Since these interactions are much smaller than the interactions between the electrons and the ligand field, they can be calculated by perturbation theory. By applying this theory, and noting that λ is negative for the Cu^{2+} ion, it is readily shown that the orbital doublet is split into two doublets by the spin–orbital interaction, and that their behaviour in a magnetic field H is described by a spin-Hamiltonian of the form

$$\mathcal{H}_{sp} = g_{\parallel}\beta H_z S_z + g_{\perp}\beta(H_x S_x + H_y S_y)$$

where, according to first-order perturbation theory, $g_{\perp} = 0$ and $g_{\parallel} = 6\alpha^2\epsilon(6, 4)$ for the lower doublet and $g_{\perp} = 0$ and $g_{\parallel} = 4 - 6\alpha^2\epsilon(0, -2)$ for the upper doublet.

Obviously, $g_{\perp}$ will be different from zero in the higher orders of perturbation theory, but it will not be large, and since the strongest perpendicular component of the EPR spectrum occurs at very high fields for low values of $g_{\perp}$, the EPR spectra of copper ions may be impossible to observe.

We shall now review the results obtained by EPR and optical spectroscopy for zeolites containing Cu^{2+} ions.

Faber and Rogers [66] were the first to report EPR spectra from Cu^{2+} ions in zeolites. They made a theoretical analysis of the hyperfine interaction constants and the g-tensor components of the EPR spectra of fully hydrated and ammonia-saturated zeolites containing Cu^{2+} ions, and they obtained data on the degree of covalency of the bond in the complexes. However, no attempt was made to identify the structure of the zeolite, evidently because the problem had not yet been formulated at the time.

Nicula and coworkers [67] studied the hydrated, partially dehydrated, and fully dehydrated forms of CuNaY zeolite. From an analysis of the spin-Hamiltonian constants, and of the temperature dependence of the EPR spectra, they showed that the copper ions in the hydrated zeolite "float" in the large holes as the hexaquo complexes.

Unlike Polák and Cerný [62], Nicula and coworkers were able to observe hyperfine splitting in partly and fully dehydrated zeolites in perpendicular as well as in parallel orientations. Using experimental spin-Hamiltonian parameters, and theoretical expressions for a tetragonal ligand field with allowance for covalent bonding [68,69], they tried to explain the observed gradual change in the spin-Hamiltonian parameters in terms of changes in the degree of covalency of σ and π bonds in the complex upon replacing water ligands by lattice oxygen atoms. This explanation is well substantiated for tetragonally distorted, octahedral Cu^{2+} complexes, but (as will be shown later) the spin-Hamiltonian parameters do not vary smoothly in practice.

These workers point out that all the observed changes in EPR spectra are reversible only in type-Y zeolites, and hence they conclude that copper-containing zeolites of type X are decomposed by vacuum heat treatment.

In this paper, also, no attempt is made to "associate" the dehydrated copper cations with any specific site in the zeolite lattice.

Richardson [70–72] has published a series of three papers devoted to an EPR study of the localisation of copper ions in type-Y zeolites containing cations of various non-paramagnetic metals. He observed EPR spectra with parameters similar to those reported by Nicula and coworkers [67], and attempted to relate them to changes in coordination of the Cu^{2+} ion during dehydration of the zeolite. However, Richardson bases all his arguments on expressions for the spin-Hamiltonian parameters of the Cu^{2+} ion in a field with C_{4v} symmetry, and tries to assign

all the observed EPR spectra for hydrated and for dehydrated samples to copper ions localised in *SII* sites, where (as stated above) the ligand field has D_{3h} symmetry (dehydrated ion) or C_{3v} symmetry (ion in an *SII* site with 1 molecule of water of hydration). Clearly, an ion on an *SII* site can have trigonally distorted octahedral surroundings only by the adsorption of three water molecules, but Richardson ignores this possibility.

Krüerke and Jung[73] also published an EPR study of copper-containing X and Y zeolites. However, their results for type-X zeolites containing copper cations should be viewed with extreme caution, since considerable doubt exists on the stability of this zeolite lattice[67].

They studied the intensity of EPR signals from samples with a high copper content (~ 20 Cu^{2+} ions per elementary cell of the zeolite) as a function of the temperature of vacuum heat treatment, and also after adsorption of water and ammonia molecules, and they showed that the intensity of the EPR signal from a fully hydrated sample does not correspond to the analytically determined concentration of copper ions. The plot of intensity of the EPR signal against dehydration temperature had a distinct minimum at 150° (~ 50% of the initial intensity). Further increase in dehydration temperature caused the signal to increase, reaching 80% of the initial intensity at 350°, but at still higher temperatures the signal once again fell off. The dehydration process was found to be reversible.

On the incorrect assumption (see above) that these large changes in the integral intensity of the EPR signal cannot be due to changes in the configuration of the ligand field close to the site of the copper cation, Krüerke and Jung explain the decreased intensity of the EPR signals during dehydration by postulating the formation of cation pairs ($S = 0.1$) in *SI'* sites of the small holes in the sodalite cell, joined by hydrogen bridges.

The increased intensity of the EPR signal on further raising the dehydration temperature was ascribed to the removal of residual water molecules, resulting in migration of the copper cations to *SI* sites and dissociation of the cation pairs.

The subsequent decrease in the intensity of the EPR signal, at dehydration temperatures above 350°, is ascribed to irreversible changes in the zeolite structure.

The most interesting of Krüerke and Jung's results were obtained with samples containing less than 8 Cu^{2+} cations per elementary cell. By analysing the shape of the absorption line they were able to establish that the parameters of the EPR spectra change in discrete jumps rather than continuously during partial dehydration of the zeolite, and they showed that two types of copper ions are present, giving EPR spectra with the following parameters:

$$\text{I}-g_{\parallel}=2.35,\ g_{\perp}=2.06,\ A=120\text{ Oe};$$
$$\text{II}-g_{\parallel}=2.31,\ g_{\perp}=2.06,\ A=175\text{ Oe}.$$

The difference between the two sets of parameters is ascribed to the existence of two possible localisation sites for Cu^{2+} ions in the zeolite, with different arrangements of nearest neighbours.

Another interesting result is the gradual decrease in total intensity of the EPR signal with increase of dehydration temperature. Krüerke and Jung admit that the ideas which they had developed for zeolites with high copper concentrations cannot be applied directly to low-concentration samples, since ion-pair formation is not likely to be significant at low concentrations.

In this context it is relevant to note that Tikhomirova and Nikolaeva[74] also proposed a non-uniform distribution of cations in the zeolite and the presence of sites with a high concentration of cations from an analysis of the individual components of the EPR spectra and their temperature dependence. However, their results relate to type-A zeolites, containing low concentrations of Cu^{2+} and Mn^{2+}.

Almost at the same time as Krüerke and Jung, Slot and Verbeck published an EPR study of zeolites (type Y) containing approximately 15 Mg^{2+}, Zn^{2+}, or La^{3+} ions and 0.3 Cu^{2+} ions per elementary cell[75]. They examined only partly or fully dehydrated samples, and they also observed two types of copper cation, with EPR spectral parameters identical to those obtained elsewhere[72,73]. From measurements of relative spectral intensities for different heat treatments they concluded that dehydration is accompanied by the gradual migration of Cu^{2+} ions into the bulk of the zeolite. They propose two explanations for the constancy of the parameters of individual EPR spectra: 1) copper ions penetrate into the interior when they are replaced (by ion exchange) by hydrated ions, and they retain their coordination when the water is removed; 2) copper ions are partly or fully dehydrated at temperatures as low as 110°, and their state is unchanged when the dehydration temperature is further increased. In both cases the migrating species are thought to be copper complexes.

The former explanation does not stand up to critical examination, since heat treatment at 400° for 72 h in an oxygen atmosphere (as in Slot and Verbeck's experiments) is known to cause practically complete dehydration of the zeolite (see, for example, Ref. 70). The second explanation seems more convincing, but it can be shown by thermal analysis (see below) that the bulk of the water is removed only at temperatures of the order of 200–300°, and therefore it is hard to accept that the coordination sphere of the copper ions is broken down at a temperature as low as 110°, and that all subsequent changes in the EPR spectrum are to be ascribed only to migration of the ions.

Slot and Verbeck ascribe the difference between the parameters of their two EPR spectra to the existence of two types of localisation sites for the ions (*SI* and *SII*). They also point out that cation migration is strongly influenced by the main cation of the zeolite.

Summarising the published results, we may conclude that for copper zeolites (unlike manganese zeolites) there is acceptable agreement between the data from different laboratories. However, contradictions are apparent in the interpretation of the results. Most workers ascribe to Cu^{2+} ions in *SI'*, *SII'*, or *SII* sites (C_{3v} tetr or C_{3v} pyram symmetry) experimental EPR spectra which clearly correspond to copper ions in ligand fields with C_{4v} symmetry. In this context, we may discuss some results obtained by the writers (in collaboration with Shvets and Pecherskaya) by EPR and optical reflection spectroscopy[76,77].

The initial samples were prepared by cation exchange of Y-zeolite in the sodium form in a solution of copper acetate, and contained 2–4 Cu^{2+} ions per elementary cell.

With hydrated samples, the results were almost identical to those previously discussed. The conclusion that in fully hydrated zeolites the copper ions are accommodated in the large holes as hexaquo complexes was confirmed by optical measurements.

In partly dehydrated (100–300°) zeolites EPR signals of two types (I and II) have also been detected. Their parameters are practically identical to those reported by other workers (signal I: $g_{\parallel} = 2.38$, $g_{\perp} = 2.08$, $A = 126$ Oe; signal II: $g_{\parallel} = 2.32$, $g_{\perp} = 2.05$, $A = 162$, $B = 22$ Oe). The optical spectra of these samples showed enhanced

optical absorption in the region 400–800 nm. On raising the dehydration temperature the relative intensity of signal II (which is absent in the EPR spectra of initial or hydrated samples, where only signals of type I can be observed) increases, and the total intensity of the EPR spectrum decreases (by a factor of 10–20 for samples fully dehydrated at 500°).

These effects were interpreted as follows[72]. The type-I EPR spectrum and the optical spectrum of a fully hydrated zeolite, consisting of one broad maximum at 800 nm, are assigned to the Cu^{2+} ion surrounded by 6 water molecules. The EPR signal of the second type is assigned to Cu^{2+} ions in a square pyramidal or a plane square coordination. This is shown by the fact that, whereas the general structure of the EPR spectrum is retained, both the ratio $\Delta g_{\parallel}/\Delta g_{\perp}$ and the optical absorption at wavelengths shorter than those for the $[Cu(H_2O)_6]^{2+}$ complex are increased. Cu^{2+} ions in these coordinations are fairly strongly bound to the zeolite lattice (apparently in SIII sites), since, in contrast to hydrated samples, their EPR spectra are the same at room temperature and at liquid nitrogen temperature.

The strong reduction in the integral intensity of the EPR signals for vacuum heat-treatment temperatures of 400 to 500° can be explained in two ways: a change in the valency state of the Cu^{2+} ions (e.g. reduction to Cu^{1+}), or a very strong broadening of the EPR lines resulting from a change in coordination. The latter explanation is the more plausible, because the initial EPR spectra can be regenerated by water adsorption at room temperature but not by heating the dehydrated samples in an oxygen atmosphere. The Cu^{2+} ions in a dehydrated zeolite are assumed to occupy sites in the planar six-membered windows of the sodalite cells of the zeolite. As stated above, the ions in these sites experience an electrical ligand field with the symmetry of a planar triangle. Under these conditions it may not be possible to observe EPR signals, because $g_{\perp}$ differs very little from zero. Relaxation may also cause broadening of the EPR line, but measurements at 4.2°K failed to reveal a new signal in the EPR spectrum.

Two papers appeared while this review was in manuscript[78,79]. Gállezot and coworkers[78] showed, by an X-ray analysis of dehydrated Cu(57%)NaY zeolite, that most of the copper ions are located in SI′ sites, where they can interact with adsorbed ammonia and pyridine molecules. The second paper[79] reports an EPR study of Cu(7%)NaY zeolite. The intensity of the spectrum is found to be constant during dehydration, and the fall of intensity observed in the writers' work is ascribed to reduction of the copper ions (as discussed above) or cation-pair formation. The formation of pairs seems improbable, particularly in samples with a low copper content, but a special study of this problem seems desirable, together with a study of the effect of oxygen on the dehydration of copper-containing zeolites.

Copper ions localised in SII sites were found to be accessible to adsorption (at room temperature) of various polar molecules (methanol, ethanol, propanol, and isopropanol)[73]. The ions appear, from EPR measurements, to remain strongly bound to the zeolite lattice near the six-membered oxygen rings (SII sites), but their coordination increases to octahedral. Decomposition of the alcohol complexes of the Cu^{2+} ions in zeolite was found to set in at temperatures of the order of 200°, accompanied by dissociation of the alcohol molecules into hydrogen and acetaldehyde (in the case of ethanol). Catalytic dehydrogenation of alcohol under normal catalytic conditions (accompanied by dehydration[21]) begins at temperatures of this order. Thus, we may conclude that Cu^{2+} ions localised in SII zeolite sites act as active centres for the catalytic decomposition of alcohol into hydrogen and acetaldehyde.

The lack of catalytic activity towards the dehydrogenation of ethanol in calcium and sodium zeolites shows that the electronic structure of the zeolite cation plays an important role in determining the specificity of the catalyst.

In this context, the work of Richardson[70] has yielded some very interesting results. It describes a comparative study, by the EPR method, of the formation of cation-radicals on different forms of zeolites (including copper) on which electron-donor molecules such as anthracene, perylene, pyrene, and naphthalene had been adsorbed. Richardson points out that zeolites containing transition-metal cations, and also cadmium cations, are much more active than other zeolites towards the electron-transfer reactions leading to the formation of cation-radicals, because of the high electron affinity and strong polarising power of these cations.

These results are entirely consistent with those of Neimark and coworkers[80], who showed (from the luminescence spectra of naphthalene adsorbed on different forms of cationated zeolites) that alkali and alkaline-earth metals lead to the formation of charge-transfer complexes between naphthalene and the zeolite lattice, followed by catalytic oxidation of the naphthalene in air to α-naphthaquinone, whereas transition-metal cations produce luminescence quenching, which the authors ascribe to direct adsorption of the naphthalene on the cation (atmospheric oxidation being thus precluded).

Zinc. The electronic configuration of the ground state of the free zinc atom is $[A](3d)^{10}(4s)^2$. Bivalent zinc ions are not paramagnetic, and are inactive in the u.v. and visible regions of the spectrum. Hence, zeolites containing Zn^{2+} ions have not been examined by either of the methods discussed in this review.

---o0o---

It is clear, from this review of the recent literature, that interesting information on the behaviour of ions of the first transition row in synthetic zeolites has been obtained by EPR and optical spectroscopy. Among the specific problems examined are the coordination and valency state of the cations after exchange and after various treatments, the sites on which ions are localised in zeolites, and the mechanism of adsorption of various molecules on these ions. In many cases, catalytically active centres have been unambiguously identified. The results on the coordination state of cations in dehydrated zeolites, and on the changes in coordination resulting from the adsorption of various compounds, are particularly interesting.

For most metals it has been reliably established that the ions enter the zeolite, during cation exchange, in the form of hexaquo complexes, which "float" fairly freely in the large holes of the sodalite cells.

Upon partial removal of the adsorbed water from the zeolite, the transition-metal ions become firmly bound to the zeolite skeleton, retaining their octahedral coordination. This reaction involves the partial replacement of the water in the coordination sphere of the ion by oxygen atoms of the zeolite lattice. Further removal of water from the coordination sphere of the ion begins (depending on the ion) at temperatures in the region of 150–250°, and goes to completion at 350–450°. The coordination of the metal

ions decreases to a square pyramid, or even to a trigonal configuration, after complete dehydration.

Unlike the alkali-metal cations, the bivalent ions of the first transition series can be stabilised in *SII* and *SII'* sites even at low extents of exchange: this effect may be due to the ability of the latter ions to form groupings of the type MOH^+. These trigonally coordinated ions (e.g. copper, cobalt, and nickel) can act as specific adsorption centres for polar molecules of water, ammonia, and alcohols. Tervalent metal ions (e.g. chromium) penetrate deep into the sodalite cell upon dehydration, and become stabilised on *SI'* sites, thus acquiring a more effective screening of their excess of positive charge by virtue of the negative charges on the zeolite lattice. Hence, these ions are relatively inaccessible to large molecules such as alcohols, aldehydes, etc.

We may also conclude from this review that contemporary workers hold conflicting views on the laws which determine the distribution of cations in zeolites. The scarcity of reliable experimental data is undoubtedly responsible for this state of affairs.

The results discussed in this review also show that synthetic zeolites provide a very interesting system for the study of the anomalous coordination states of transition-metal cations introduced into the zeolite by cation exchange. These ions (particularly when doubly charged) act as adsorption centres for a number of molecules; the possibility that the molecules thus coordinated are chemically activated and that the resulting catalytic properties of transition-metal ions can be exploited is a very interesting topic, which lies beyond the scope of the present review.

REFERENCES

1. J. Turkevich, Catalysis Rev., 1, 1 (1967).
2. Kh. M. Minachev, V. I. Garanin, and Ya. I. Isakov, Uspekhi Khim., 35, 12 (1966) [Russ. Chem. Rev., No. 1 (1966)].
3. P. B. Venuto and P. S. Landis, Adv. Catalysis, 18, 259 (1968).
4. J. Turkevich and J. Ono, Adv. Catalysis, 20, 135 (1969).
5. D. J. Yates, Catalysis Rev., 2, 113 (1969).
6. R. M. Barrer, J. W. Baunham, F. W. Bultitude, and W. M. Meier, J. Chem. Soc., 195 (1959).
7. J. Selbin and R. Mason, J. Inorg. Nuclear Chem., 20, 222 (1961).
8. N. F. Ermolenko, S. A. Levina, and L. B. Pansevich-Kolyada, Dokl. Akad. Nauk Beloruss.SSR, 394 (1964).
9. N. F. Ermolenko and L. V. Pansevich-Kolyada, Symposium "Tseolity, Ikh Sintez, Svoistva, i Primenenie" (Zeolites—Synthesis, Properties, and Applications), Izd. Nauka, Moscow–Leningrad, 1965, p. 171.
10. I. E. Neimark, M. A. Piontkovskaya, et. al., Symposium "Tseolity, Ikh Sintez, Svoistva, i Primenenie" (Zeolites—Synthesis, Properties, and Applications), Izd. Nauka, Moscow–Leningrad, 1965, p. 146.
11. M. M. Dubinin, Z. A. Zhukova, and N. V. Kel'tsev, Symposium "Sinteticheskie Tseolity" (Synthetic Zeolites), Izd. Akad. Nauk SSSR, Moscow, 1962, p. 7.
12. I. E. Neimark, A. I. Rastrenenko, V. P. Fedorovskaya, and A. S. Plachinda, Symposium "Sinteticheskie Tseolity" (Synthetic Zeolites), Izd. Akad. Nauk SSSR, Moscow, 1962, p. 46.
13. P. C. Hyang, A. Mizany, and J. L. Paully, J. Phys. Chem., 68, 2575 (1964).
14. R. M. Barrer and W. M. Meier, Trans. Faraday Soc., 54, 1074 (1958).
15. N. F. Ermolenko, L. P. Shirinskaya, and M. V. Zaretskii, Izv. Akad. Nauk Beloruss.SSR, Ser. Fiz.-Tekh. Nauk, 1963, 111.
16. G. M. Panchenkov and A. M. Tolmachev, Kinetika i Kataliz, 4, 853 (1963).
17. G. M. Panchenkov, A. M. Tolmachev, and V. A. Fedorov, Zhur. Fiz. Khim., 37, 456 (1963) [Russ. J. Phys. Chem., No. 2 (1963)].
18. A. M. Tolmachev, V. A. Fedorov, and G. M. Panchenkov, Zhur. Fiz. Khim., 37, 2548 (1965) [Russ. J. Phys. Chem., No. 10 (1965)].
19. L. L. Ames, Jnr., J. Inorg. Nuclear Chem., 27, 885 (1965).
20. D. W. Breck, J. Chem. Educ., 41, 678 (1964).
21. J. A. Rabo, C. L. Angell, and V. Schomaker, "Proceedings of the Fourth International Congress on Catalysis", Moscow, 1968, Paper No. 54.
22. K. Ballhausen, "Introduction to Ligand Field Theory" (Translated into Russian), Izd. Mir, Moscow, 1964.
23. I. B. Bersuker and A. V. Ablov, "Khimicheskaya Svyaz' v Kompleksnykh Soedineniyakh" (The Chemical Bond in Complex Compounds), Kishinev, 1962.
24. V. A. Shvets and V. B. Kazanskii, Symposium "Kompleksoobrazovanie v Katalize" (Complex Formation in Catalysis), Izd. Nauka, 1968, p. 217.
25. G. A. Sinyukova, I. D. Mikheikin, and K. I. Zamaraev, Strukturnaya Khim., 2, 23 (1970).
26. A. Abragam and M. H. L. Pryce, Proc. Roy. Soc., A 205, 135 (1951).
27. M. M. Selim, Thesis, Moscow, 1968.
28. A. L. Nicula, Rev. Chim. (Acad. R. P. R.), 19, 129 (1968).
29. C. K. Jorgensen, "Absorption Spectra and Chemical Bonding in Complexes", Pergamon Press, Oxford, 1962.
30. Yu. S. Khodakov, I. D. Mikheikin, V. S. Nakhshunov, V. A. Shvets, V. B. Kazanskii, and Kh. M. Minachev, Izv. Akad. Nauk SSSR, Ser. Khim., 523 (1969).
31. J. V. Smith, J. M. Bennett, and E. M. Flanigen, Nature, 215, 241 (1967).
32. M. V. Urushadze and G. V. Tsitsishvili, Kinetika i Kataliz, 11, 1080 (1970).
33. T. J. Barry and L. A. Lay, J. Phys. Chem. Solids, 27, 1821 (1966).
34. J. C. M. Henning, J. Liebertz, and R. P. Van Stapele, J. Phys. Chem. Solids, 28, 1109 (1967).
35. I. D. Mikheikin, O. I. Brotikovskii, and V. B. Kazanskii, Kinetika i Kataliz, 13, No. 2 (1972).
36. B. Bleaney, Phil. Mag., 42, 441 (1951).
37. B. Bleaney and R. S. Rubins, Proc. Phys. Soc., Lond., 77, 103 (1961).
38. B. Bleaney and R. S. Rubins, Proc. Phys. Soc., Lond., 78, 778 (1961).
39. J. Ursu and A. Nicula, Rev. Roum. Phys., 9, 343 (1964).
40. T. J. Barry and L. A. Lay, Nature, 208, 1312 (1965).
41. T. J. Barry and L. A. Lay, J. Phys. Chem. Sol., 29, 1395 (1968).
42. N. N. Tikhomirova and L. G. Dzhashiashvili, Zhur. Strukturnoi Khim., 7, 886 (1966).
43. L. G. Dzheshiashvili, N. N. Tikhomirova, and G. V. Tsitsishvili, Zhur. Strukturnoi Khim., 8, 453 (1967).
44. L. G. Dzhashiashvili, N. N. Tikhomirova, and G. V. Tsitsishvili, Zhur. Strukturnoi Khim., 10, 443 (1969).
45. R. Stahl-Brada and W. Low, Phys. Rev., 116, 561 (1959).

46. V.I. Gol'danskii, I. P. Suzdalev, A. S. Plachinda, and L. G. Shtyrkov, Dokl. Akad. Nauk SSSR, 169, 872 (1966).
47. V.I. Gol'danskii, I. E. Neimark, A. S. Plachinda, and I. P. Suzdalev, "Proceedings of the Fourth International Congress on Catalysis", Moscow, 1968, Symposium III, Novosibirsk, Preprint No. 16.
48. L. V. Skalkina, Thesis, Moscow, 1970.
49. J. A. Morice and L. K. C. Rees, Trans. Faraday Soc., 64, 1388 (1968).
50. W. N. Delgass, R. L. Garten, and M. Boudart, J. Phys. Chem., 73, 2970 (1969).
51. F. Cotton and D. Wilkinson, "Modern Inorganic Chemistry" (Translated into Russian), Izd. Mir, Moscow, 1969.
52. A. Abragam and M. H. L. Pryce, Proc. Roy. Soc., A 206, 173 (1951).
53. J. Owen and K. D. Bowers, Reports Progr. Phys., 18, 304 (1955).
54. L. S. Singer, J. Chem. Phys., 23, 379 (1955).
55. F. Wolf et al., Chem. Tech. (Berlin), 18, 339 (1966).
56. K. Klier, J. Amer. Chem. Soc., 91, 5392 (1969).
57. I. D. Mikheikin, O. I. Brotikovskii, G. M. Zhidomirov, and V. B. Kazanskii, Kinetika i Kataliz, 12, 1442 (1971).
58. J. A. Rabo, C. L. Angell, R. H. Kasai, and V. Schomaker, Discuss. Faraday Soc., 41, 328 (1966).
59. D. H. Olson, J. Phys. Chem., 12, 4366 (1968).
60. J. A. Rabo, P. E. Pickert, E. Dempsey, and V. Schomaker, "Proceedings of the Third International Congress on Catalysis", Amsterdam, 1964, Vol. 1, p. 714.
61. D. H. Olson, G. T. Kokotailo, and J. F. Charnell, Nature, 215, 270 (1967).
62. R. Polák and V. Cerný, J. Phys. Chem. Solids, 29, 945 (1968).
63. K. Klier and M. Ralek, J. Phys. Chem. Solids, 29, 951 (1968).
64. D. J. C. Yates, J. Phys. Chem., 69, 1676 (1965).
65. A. M. Rubinshtein, Kh. M. Minachev, A. A. Slinkin, V. I. Garanin, and G. A. Ashavskaya, Izv. Akad. Nauk SSSR, Ser. Khim., 786 (1968).
66. R. J. Faber and M. T. Rogers, J. Amer. Chem. Soc., 81, 1849 (1959).
67. A. Nicula, D. Stamires, and J. Turkevich, J. Chem. Phys., 42, 3684 (1965).
68. J. Owen, Proc. Roy. Soc., A 227, 183 (1955).
69. R. Neiman and D. Kivelson, J. Chem. Phys., 35, 149, 156, 162 (1961).
70. J. T. Richardson, J. Catalysis, 9, 172 (1967).
71. J. T. Richardson, J. Catalysis, 9, 178 (1967).
72. J. T. Richardson, J. Catalysis, 9, 182 (1967).
73. U. Krüerke and P. Jung, Z. phys. Chem. (Frankfurt), 58, 53 (1968).
74. N. N. Tikhomirova and I. V. Nikolaeva, Zhur. Strukturnoi Khim., 10, 547 (1969).
75. H. B. Slot and J. L. Verbeck, J. Catalysis, 12, 216 (1968).
76. I. D. Mikheikin, V. A. Shvets, and V. B. Kazanskii, Kinetika i Kataliz, 11, 747 (1970).
77. I. D. Mikheikin, Yu. I. Pecherskaya, and V. B. Kazanskii, Kinetika i Kataliz, 12, 191 (1971).
78. P. Gállezot, Y. Ben Taarit, and B. Imelik, Compt. rend., (C), 272, 261 (1971).
79. C. Nacchache and Y. Ben Taarit, Chem. Phys. Letters, 11, 11 (1971).
80. A. M. Eremenko, E. F. Shcheka, M. A. Piontovskaya, and I. E. Neimark, Tekh. Eksper. Khim., 242 (1969).

Zelinskii Institute of Organic Chemistry
of the USSR Academy of Sciences,
Moscow